Tsunami simulations of the 1867 Virgin Island earthquake: Constraints on epicenter location and fault parameters

Roy Barkan[a] and Uri ten Brink[b,*]

[a] *Department of Geophysics and Planetary Sciences, Tel Aviv University, Ramat Aviv, Tel-Aviv 69978, Israel*

[b] *U.S. Geological Survey, Woods Hole, MA 02543, USA*

* Corresponding author: Uri ten Brink, USGS Woods Hole Science Center, 384 Woods Hole Rd., Woods Hole, MA 02543 USA. Tel: +1-508-457-2396; Fax: +1-508-457-2310; *E-mail address:* utenbrink@usgs.gov

Abstract

The November 18th, 1867 Virgin Island earthquake and the tsunami that closely followed caused considerable loss of life and damage in several places in the northeast Caribbean region. The earthquake was likely a manifestation of the complex tectonic deformation of the Anegada Passage, which cuts across the Antilles island arc between the Virgin Islands and the Lesser Antilles. In this study, we attempt to characterize the 1867 earthquake with respect to fault orientation, rake, dip, fault dimensions, and first tsunami wave propagating phase, using tsunami simulations that employ high-resolution multibeam bathymetry. In addition, we present new geophysical and geological observations from the region of the suggested earthquake source. Results of our tsunami simulations based on relative amplitude comparison limit the earthquake source to be

along the northern wall of the Virgin Islands Basin, as suggested by Reid and Taber (1920), or on the carbonate platform north of the basin, and not in the Virgin Islands Basin, as commonly assumed. The numerical simulations suggest the 1867 fault was striking 120°-135° and had a mixed normal and left-lateral motion. First propagating wave phase analysis suggests a fault striking 300°- 315° is also possible. The best fitting rupture length was found to be relatively small (50 km), probably indicating the earthquake had a moment magnitude of ~7.2 . Detailed multibeam echosounder surveys of the Anegada Passage bathymetry between St. Croix and St. Thomas reveal a scarp, which cuts the northern wall of the Virgin Islands basin. High-resolution seismic profiles further indicate it to be a reasonable fault candidate. However, the fault orientation and the orientation of other sub-parallel faults in the area are more compatible with right-lateral motion. For the other possible source region, no clear disruption in the bathymetry or seismic profiles was found on the carbonate platform north of the basin.

Keywords: Tsunami modeling, 1867 Virgin Island tsunami, Anegada Passage.

---

1. Introduction

The 1867 Virgin Islands earthquake and tsunami is an example of a natural disaster, which changed the course of local history. At the time of the event, the U.S. was engaged in the purchase of the then Danish Virgin Islands and had sent three navy ships to explore the islands. The devastating tsunami, which caused loss of lives and damage to the navy ships was among the reasons that the purchase was postponed for another 50 years (e.g., Dookhan, 1975). However, the presence of navy ships in St. Thomas and St. Croix at the time of the earthquake and tsunami has also resulted in relatively accurate

reports by the ships' commanding officers of water level and timing of events. Reid and Taber (1920) summarized these reports and used them to locate the possible epicenter between St. Thomas and St. Croix. The November 18, 1867 earthquake consisted of two main shocks, about 10 minutes apart in the same general area (Reid and Taber, 1920). The shaking was most severe in St. Thomas and almost as severe in St. Croix. Reid and Taber (1920) estimated earthquake intensity IX (using Rossi-Forel scale) at these two islands and at Tortola, St. John, Vieques, and Culebra and lower intensity in eastern Puerto Rico, Virgin Gorda, and the northern Lesser Antilles. A tsunami wave closely followed the shocks and had significant effects in Puerto Rico, The Virgin Islands, the Lesser Antilles and Venezuela (Table 1 and Fig. 1; Reid and Taber, 1920; Zahibo et al., 2003; O'Loughlin and Lander, 2003). With the exception of Guadeloupe, the highest run-up reports were from St. Thomas and western St. Croix.

The 1867 earthquake is likely a manifestation of tectonic deformation of the Anegada Passage. The Anegada Passage cuts across the Antilles arc between the Virgin Islands and the Lesser Antilles. It is the only deep-water passage between the Atlantic Ocean and the Caribbean Sea, where Atlantic intermediate water can enter the Caribbean (Fratantoni et al., 1997). The passage has a complex bathymetry with irregular ridges reaching 40 m b.s.l. and irregular basins reaching a depth of 4500 m. (Fig. 1). Relative motion across the Anegada Passage has been suggested to be left-lateral transtension (Hess and Maxwell, 1953; Gill, 1999; ten Brink, 2005), perpendicular extension (Murphy and McCann, 1979), or right-lateral transtenstion (Jany et al., 1990) but earthquake activity and geodetic GPS data have hitherto been too low to define the sense and rate of motion. Hence, defining the rupture parameters of the 1867 earthquake may help constrain the motion across the Anegada Passage.

A few attempts have been made to characterize the 1867 earthquake based on the orientation of the wall of the Virgin Islands basin, tsunami arrival time, earthquake shaking intensity and numerical modeling of the tsunami (Reid and Taber, 1920; Lander et al. 2002; Zahibo et al., 2003). The origin of the earthquake is most commonly assumed to be in the Virgin Islands basin between St. Croix and St. Thomas, (Fig. 1). Two major solution faults were previously proposed and will be referred to later on in this paper as:

Reid Fault (RF) - Reid and Taber (1920) suggested an epicenter located on the north wall of the Virgin Island Basin not far from latitude 18.16667°N and longitude 65.0°W (epicenter 14 in Figs. 1 and 2). They hypothesized an EW trending fault, several 10s of km long, located 16-17 km south of St. Thomas along the northern wall of the Virgin Islands Basin and having a slip < 10 m, as a possible candidate.

Zahibo Fault (ZF) - Zahibo et al. (2003) suggested a 120x30 km thrust fault (rake of 90°) located within the Virgin Islands Basin at 18.0°N and 65.0°W and oriented N75°E (epicenter 7 in Figs. 1 and 2). The dip angle, focal depth, and displacement selected for their hydrodynamic modeling were 70°, 3000 m, and 8 m respectively.

In this study, we first constrain the epicenter of the 1867 earthquake using tsunami simulations that utilize newly collected high-resolution multibeam bathymetry (refer to section 2 for more details). Features such as fault orientation, rake, dip, and fault dimensions are then tested, taking into account empirical relationships between earthquake magnitude and fault parameters, relative plate motion, and first wave propagating phase. Finally, we present geophysical and geological observations from the region of the suggested earthquake source and discuss locations of possible faults and their relationship to the overall tectonic deformation of the Anegada Passage.

Constraining source location and fault parameters based on tsunami travel time is problematic (Zahibo, 2003; Barkan et al., 2009) due to the inaccuracy of historical reports, due to the possibility of localized landslide-generated tsunamis triggered by the earthquake, and due to the difficulties in simulating tsunami propagation at shallow depths (see sections 2.1 and 2.2 below). The exact time of the 1867 earthquake is uncertain. Reports indicate it was between 14:30-15:00 o'clock (Reid and Taber, 1920; O'Loughlin et al., 2003). For a tsunami traveling in deep water (i.e., the long-wavelength limit) at a phase speed of $\sqrt{gh}$ (g being the acceleration due to gravity and h is the water depth), such a difference in origin time makes correlation between simulated arrival times and historical arrival times highly inaccurate. Furthermore, Reid and Taber (1920) suggested that the unreasonably-high reported run-up at Guadeloupe and seemingly immediate arrival time of the tsunami (15:00) may be attributed to a nearby landslide. Zahibo et al. (2003) agree with this suggestion arguing that the report in Guadeloupe was a result of a local amplification of the wave. Because of the above reasons, direct constraining of source location and fault parameters based on tsunami travel time was not attempted in this study. Nevertheless, the tsunami arrival times depicted in the marigrams generated from the simulated RF (Table 1, Calculated Travel Time) are reasonable with respect to historical arrival time reports (Table 1, Reported Travel Time).

2. Methodology

2.1 Tsunami model simulations

All simulations presented in this study were generated using COMCOT (Cornell Multi-grid Coupled Tsunami Model; Liu et al., 1998; Lynett et al., 2002). COMCOT solves both linear shallow water (LSW) and non-linear shallow water (NLSW)

equations in spherical coordinates. Aside from the governing equations, the linear vs. non-linear hydrodynamic models, as implemented in COMCOT, also differ in the coastal boundary conditions. The linear model uses reflective boundary conditions and is therefore unable to perform explicit run-up calculations at the shallow water areas along the coast. The COMCOT non-linear model uses moving boundary conditions and is capable of more accurate wave amplitude calculations closer to shore. The latter model was therefore used in this study. In principle, numerical computation of wave heights based on shallow water equations is sufficient and accurate as long as the modeled tsunami wavelength is much greater than water depth and the wave amplitude is much smaller than water depth. This principle holds up until the deep part of the continental shelf. Consequently, this study is unable to provide definite run-up results and only relative amplitudes can be considered.

The input depth file contains the bathymetry of the region where the simulation took place. Tsunami propagation is highly influenced by sea floor bathymetry (e.g., Matsuyama et al., 1999; Mofjeld et al., 2000). High-resolution bathymetric grids are therefore essential for accurate modeling. Two different bathymetric grids were used for all simulations; a 394x476 bathymetry grid (LRES) with 1 arcmin resolution covering the entire area of interest (-67.052067°W to -60.4723°W and 11°N to 18.933°N) (LRES- Shaded blue bathymetry; Fig. 1a), and an overlapping 415x840 bathymetry grid (HRES) with 12 arcsec resolution covering the near source area (-67.035005°W to -64.2354°W and 17.5166015°N to 18.8999°N) (HRES- Multibeam bathymetry; Fig. 1b). The output file used for all interpretations in this study is the maximum wave amplitude file. This file contains the calculated maximum sea level amplitude for a selected region, throughout an entire simulation run (tsunami propagation time of 95 minutes or 5700 1-

sec time steps).

2.2 Tsunami amplitude

To calculate wave amplitude, we averaged the amplitudes of 5 or 9 model grid points at shelf locations: 3 (or 5) adjacent points lined in a north-south direction and 3 (or 5) adjacent points lined in an east-west direction, with common center points, whose coordinates are listed in Table 1. Points with zero wave amplitude or a depth shallower than 9 m were discarded from the average calculations. The groups of calculated points consisted of five points at sites located in the Lesser Antilles where only the LRES grid was available, and nine points at sites in the Virgin Islands and Puerto Rico, where the HRES grid was available. Because tsunami amplitude is strongly dependent on water depth (Liu et al., 1998; Ward, 2002) all amplitudes were normalized to depths of 40 m and 100m prior to averaging using Green's law (Green, 1837):

(1) $$h_1 = \left(\frac{b_0}{b_1}\right)^{1/2} \left(\frac{d_0}{d_1}\right)^{1/4} \cdot h_0$$

where d_0 and b_0 are the water depth at the location and the angular section width of the propagating wave, d_1 and b_1 are the water depth and the angular section width at the site where the wave amplitude is to be approximated (40 m and 100m in this case), and h_0 and h_1 are the corresponding wave amplitudes at these two locations. Because the distance between the computed and approximated locations in this study was reasonably short, the angular section width of the propagating wave was considered to remain constant and equation (1) reduces to:

(2) $$h_1 = \left(\frac{d_0}{d_1}\right)^{1/4} \cdot h_0$$

168 The normalization of wave heights following equation (2) ensures a reliable comparison
169 between the sites.
170
171 *2.3 A method to quantitatively compare between possible epicenters and fault rupture*
172 *parameters*
173 Direct comparison between historical tsunami run-up reports and hydrodynamic
174 model predictions with different epicenters and fault rupture parameters is difficult for
175 the following reasons. First, historical eyewitness reports are not always reliable, second,
176 our model does not calculate actual run-ups (see section 2.1) and third, run-up is sensitive
177 to near shore bathymetry and on shore topography. To overcome these limitations, the
178 following method was used.
179 Estimated sea level changes (by officers on moored U.S. naval ships in Charlotte
180 Amalie and Frederiksted harbors) and run-ups (by eyewitnesses on shore) of the 1867
181 tsunami were used for the analyses (Reid and Taber, 1920; Zahibo et al., 2003;
182 O'Loughlin and Lander, 2003). All observed run-up heights were scaled to Hassel Island
183 at the entrance of Charlotte Amalie harbor, St. Thomas, because of the elaborate and
184 consistent U.S. naval reports from that location (Reid and Taber, 1920; O'Loughlin and
185 Lander, 2003). In order to account for the magnifying effect that harbors have on tsunami
186 amplitude we used the ratio between Charlotte Amalie (inside harbor) to Hassel Island
187 (outside harbor) given by the naval reports as an empirical magnification ratio for all
188 other historical locations. (Different harbor responses will of course have slightly
189 different magnifications, but in the absence of information from other harbors, we use a
190 single ratio). All Run-ups reported inside the harbor (St. Croix for instance) were
191 decreased using the above ratio to give the 'outside harbor' amplitude. The 'outside

192 harbor' amplitudes were later compared to that of St. Thomas and are depicted in Table 1
193 (Relative Amp. (X^2)). In order to quantitatively determine which epicenter best fits the
194 historical reports with respect to location, fault strike, fault rake, and fault dimensions, we
195 used a Chi-Squared minimization scheme,

196 (3) $$X_i^2 = \sum_{j=1}^{10} (Amp_{table_j} - \frac{Amp_j^i}{Amp_0^i})^2 / Amp_{table_j}$$

197 where *i* represents the 21 model epicenter locations (Figure 1 and table 2). Amp_{table_j}
198 is the relative amplitude (X^2) reported at location j (see column 'j' in Table 1). These 10
199 locations along the coasts were chosen because the historical run-up reports at these
200 locations were consistent among sources (Reid and Taber, 1920; Zahibo et al., 2003;
201 O'Loughlin and Lander, 2003). Amp_j^i is the amplitude generated by epicenter *i* at site *j*
202 and Amp_0^i is the calculated amplitude at Hassel Island, St. Thomas. The best fitting
203 source should minimize the Chi Squared value.

204 Chi Squared values calculated when depth was normalized to 40 m and 100 m
205 showed similar results, Figures 3-5 were created using equation 3 for amplitudes
206 normalized to 40 m.

207

208 **3. Results and Discussion**

209 Figure 1 and Table 2 show and list all 21-earthquake sources that were modeled. All
210 fault parameters roughly matched the empirical relationships depicted in Wells and
211 Coppersmith (1994) for an M_W 7-7.5 earthquake. The initial perturbation of sea surface
212 height was assumed to be similar to the sea floor perturbation from a calculated elastic
213 dislocation model of fault rupture. The upper end of the fault plane was assumed to reach

1 km below the surface to avoid singularities in the rupture surface. The rake and strike angles follow Aki and Richards's convention (1980).

3.1 Source location

The first set of simulations was designed to constrain the fault location. A fault strike of 110° was chosen for these simulations, which is the orientation of a suspected fault along the northern wall of the basin, shown in the multibeam bathymetry data as an interruption to the canyon system (heavy dashed line marked 1867? in Fig. 2). Figure 3 compares source locations at different longitudes and latitudes based on the method outlined in Section 2.3 and indicates that the best-fit source is located around 65°W and 18.1667-18.3N. In other words, the best source location is along the northern wall of the Virgin Islands Basin, as suggested by Reid and Taber (1920), or on the carbonate platform north of the basin. The northern wall of the Virgin Island Basin is also associated with micro-seismic activity, whereas the floor of the basin and its southern wall are not (Murphy and McCann, 1979, PRSN). Two shallow (~15 km) earthquake swarms occurred in Nov. and Dec. 1978 at 18.1°N 64.9°W (Frankel et al., 1980), which is close to the morphological expression of the possible 1867 rupture (yellow star in Fig. 2).

3.2 Fault Parameters: strike, rake, fault dimensions and earthquake magnitude

The second set of simulations was designed to examine possible fault parameters based on the criteria developed in Section 2.3. A fault located at source 14 (RF; Fig. 1 and 2 and Table 2) was chosen for this set because it is the southernmost epicenter in the group of favorable epicenters, determined in the previous section (Fig. 3b). As such it

minimized topographic interference by islands when we tested different fault orientations. In order to determine possible strike orientations, the fault strike was rotated between 65° - 140°. Figure 4a shows that fault strikes ranging from 120°- 140° fit better than the previously suggested E-W trending RF and ZF. Figure 4b shows a comparison between different fault dimension combinations (Length x Width x Slip) which yield a ~7.5 Mw earthquake. McCann (1985) suggested a surface wave magnitude, Ms=7.5, based on Reid and Taber (1920) observations of similar intensity and maximum felt distance for the 1867 Virgin Islands earthquake and for the 1918 western Puerto Rico earthquake and based on his magnitude estimate of M=7.5 for the 1918 earthquake. From this analysis, a smaller fault area with larger slip (combination #3), i.e., a larger stress drop, best fits the historical reports. Empirical relationships (Wells and Coppersmith, 1994) indicate that the length and width of the fault in combination #3 fit a smaller magnitude earthquake (M7.2). The suggested slip of 6 m fit a Mw~7.5 earthquake according to the same empirical relationships. However, the log-linear correlation between average displacement (slip) and earthquake magnitude (Wells and Coopersmith, 1994) is much weaker (r = 0.75) and has a larger standard deviation (s = 0.36) than the correlation between rupture length or rupture width and magnitude (r = 0.94, 0.84, s = 0.16, 0.15). Therefore, using fault length and width to estimate the 1867 earthquake magnitude is probably more reliable than using its slip, indicating that the magnitude might have been closer to M7.2. This conclusion agrees with later analyses of the 1918 western Puerto Rico earthquake, which revised its magnitude to Ms=7.3 (Pacheco and Sykes, 1992) and Mw=7.2 (Doser (2005).

Figure 4c compares between different fault rakes. The best-fit fault rake has an equal mix of strike slip and normal component (-45°), which is in agreement with previous

suggestions of left-lateral transtension (ten Brink, 2005) and perpendicular extension (Murphy and McCann, 1979). However, fault orientation and the orientation of other faults in the area (Fig. 2) are more compatible with a mixed right-lateral and normal faulting. Additional analysis of bathymetry, seismic reflection and GPS data is required to better define the regional deformation pattern.

3.3 The 1867 earthquake suggested epicenter and fault parameters.

Table 3 summarizes the parameters of the two best fitting faults (RF, NF) and the previously suggested ZF. Figure 5 compares their Chi squared fit to observations with the previously determined source fault from hydrodynamic models (Zahibo et al., 2003). Both RF and NF are better fit than ZF. Although it appears that ZF is a better candidate with respect to reported tsunami sites farther away in the Lesser Antilles (bold numbered sites 4-10 in Table 1) RF and NF are much better candidates with respect to sites in the US Virgin Islands and Puerto Rico (gray shaded sites 0-3 in Table 1). In both simulated RF and NF a SE striking fault (120°, 135°) fits better than a NW striking fault (300°, 315°) indicating that the NE part of the fault was uplifted. Figure 6 shows plots of maximum sea level from RF, illustrating what the 1867 tsunami might have looked like. Table 1 (Relative Amp. (Calc.)) lists maximum sea levels from RF at the historical locations used for comparison in this study. Plots and values from NF are very similar. Note the high wave amplitude along the south shore of Vieques in agreement with Reid and Taber (1920) report that "Immediately after the shock a high wave broke on the south side of Viequez, and later washed its northern shore". There could be several reasons why tsunami deposits from the 1867 were not found in core analysis from Lagoona Playa Grande (Woodruff et al., 2008) tsunami deposits in on the southwest coast

of the island (LPG in Fig. 2) (J. Woodruff, pers. Comm.., 2009), First, Woodruff et al. could not differentiate between deposits from tsunamis and hurricane. Second, there were many events during the past 200 years, but only two category 5 hurricanes (1899 and 1963) could be identified in the cores with certainty. The 1899 deposits could be mixed with the 1867 deposits. Third, the 1867 tsunami followed three weeks after a category 4 hurricane in the area. Finally, the barrier between the lagoon and the sea is 2-3 m high, and the lagoon is located at the western edge of the calculated flooded coast (compare Fig.2 and 6) beyond the wide platform south of Vieques.

Figures 7 and 8 show the marigrams from RF and NF respectively, in places along the Caribbean and the Lesser Antilles shown in Table 1 and Figure 1 including St. Thomas**.** In all marigrams for RF and NF, the leading propagating wave is a depression phase (ocean withdrawal), followed by an elevation phase (flooding), in agreement with observations (Reid and Taber 1920, O'Loughlin, 2003). The marigrams shown in Zahibo, 2003 indicate a leading elevation phase in most of the locations tested, further undermining the proposed epicenter location and suggested thrust motion.

Figure 9 shows that for marigrams generated from RF with a strike of 300° the leading propagating wave in all sites is a depression phase as well. The marigram for St. Thomas shows an immediate withdrawal, which is compatible with two eyewitness reports cited by Reid and Taber (1920). We are therefore, unable to determine whether the SW side of the fault was the one to drop due to the earthquake (strike 120°) or vice versa (strike 300°) based on the marigrams. In addition, although the bathymetry of the basin is more compatible with a drop of the SW side of the fault, the tilted strata at the eastern tip of Vieques and the presence of El-Seco promontory are more compatible with a rising SW side of the fault. Seismic profiles across the fault (Fig. 10) are inconclusive.

3.4 Geophysical evidence for the 1867 earthquake suggested epicenter

RF is located only 7 km north of a potential active fault observed in geological and geophysical data (Heavy dashed line marked 1867? in Fig. 2). The surface expression of the fault is oriented 110°. It is a hanging valley, which cuts the northern wall of the Virgin Islands basin diagonally, and which disrupts the drainage system along the basin wall. The valley, A 15x10 km area of the wall below the hanging valley appears disrupted in the bathymetry (Fig. 2) and in crossing seismic lines (Fig. 10). This hanging valley may be the surface expression of the 1867 rupture. It may continue northwestward onto the shelf isolating a promontory (El-Seco in Fig. 2). The fault trace may reach the northern side of the eastern tip of Vieques, where a tilted Pleistocene (?) carbonate platform is uplifted (Vaughan, 1923; Meyerhoff, 1927). However, mulitbeam bathymetry (Fig. 3) and seismic profiles on the shelf (not shown) do not show a fault scarp between Vieques and El-Seco promontory, or anywhere else on the shelf between St. Thomas, Cuelebra, and Vieques. The lack of morphological and geophysical evidence for a fault rupture on the shelf may be due to the high rate of coral growth (1-1.5 m/100 y; Macintyre et al., 1977; van Moorsel, 1985) or the fact that not the entire fault ruptures the surface (Wells and Coopersmith, 1994).

Donnelly (1966) proposed the presence of an active fault at orientation of 345° with a drop on the NE side crossing the shelf in the vicinity of Sail Rock (marked DF in Fig. 2). Multibeam bathymetry, high-resolution seismic profiles, and a dive have failed to identify a fault, and the step in the sea floor disappears 8 km south of Sail Rock and does not reach the shelf edge (Fig. 2).

Other lineated disruptions in the morphology of the basin can be detected in the multibeam bathymetry map (Fig. 2), Although one of these morphological lineaments could give rise to a strong second tremor ~10 minutes after the first tremor (Reid and Taber, 1920), their locations could not generate the observed tsunami (Fig. 3).

Seismic reflection profiles across the Virgin Islands Basin show an asymmetric sediment fill, which thickens to the south (Fig. 10). This would indicate that throughout geologic history, the southern boundary of the basin could have been significantly more active than the northern boundary. However, presently, micro-seismic activity is centered along the northern wall of the basin (Frankel et al., 1980; Puerto Rico Seismic Network catalog), and the source of the 1867 tsunami appears to have been along that side of the basin. In addition, the deepest depression of Anegada Passage (-4533 m) is located at the base of the northern wall of the Virgin Islands basin and may have a geometric relationship to the proposed faults on the northern wall of the basin (Fig. 2). In contrast to the northern wall of the basin, the southern wall of the basin appears to be shaped by large landslide scars (Fig. 1b). The complex fault pattern of Anegada Passage between longitudes 63.5°-66°W further suggests changes in the locus of fault activity in this area through time.

4. Conclusions

Methodological tsunami simulations based upon historical reports of the 1867 Virgin Island tsunami suggest the following conclusions. First, the earthquake epicenter seems to have been along the upper part of the northern wall of the Virgin Islands Basin between St. Croix and St. Thomas as previously proposed by Reid and Taber (1920). The two best fitting epicenter locations are RF: -65W, 18.1667N (following Reid and

Taber, 1920) and NF: -65W, 18.2N. NF is a better fitting fault location for far sites along the Lesser Antilles and RF is better fitting for nearer sites in the Virgin Islands and Puerto Rico. The most favorable fault source strikes are 120° for RF and 135° for NF, in contrast to the previously suggested 65°-90° trending faults (Reid and Taber, 1920; Zahibo et al., 2003). Such strikes are compatible with a drop in the SW side of the fault. Simulated marigrams, the region's bathymetry and seismic profiles however, suggest fault strikes of 300° and 315° (a drop in the NE side of the fault) are also possible. No attempt was made in this study to combine the two suggested fault ruptures [RF and NF] to a single fault, which might have yielded better results. The best fitting rake for both RF and NF is -45° (LL/N) which is in agreement with several previous relative plate motion studies in the region. However, fault geometry deduced from detailed multibeam bathymetry is more compatible with a regional mixed right-lateral and normal faulting. In addition, the best fitting fault slip is relatively large, further indicating that the focal mechanism had a normal component. The best fitting fault area is relatively small, probably indicating the earthquake had a moment magnitude of ~7.2. Marigrams of both RF and NF show that the first arrival wave phase in all places was a depression, in agreement with historical reports. A detailed mulitbeam survey of the Anegada Passage bathymetry between St. Croix and St. Thomas reveals a hanging valley, which may correspond to our hypothesized RF (Fig. 2 and 3). The valley is oriented 110°, cuts the northern wall of the Virgin Islands basin diagonally, and disrupts the drainage along the basin wall. No clear scarp in the bathymetry was found to support our hypothesized NF in either the multibeam bathymetry or in high-resolution seismic profiles (e.g., Fig. 2).

It is important to note that the interpretations in this report considered relative amplitudes only and that high-resolution near-shore bathymetry was only available for

the Virgin Islands and Puerto Rico region. High-resolution bathymetry of the Lesser Antilles is crucial for more accurate run-up calculations and better analysis of the possible epicenter location and fault parameters.

Data and resources

Propagation models were calculated using the Cornell Multi-grid Coupled Tsunami Model (COMCOT) developed by P.L.-F. Liu, X. Wang, S-B. Woo, Y-S. Cho, and S.B. Yoon, at the School of Civil and Environmental Engineering, Cornell University (Liu et al., 1998). All calculations were performed on the Arctic Region Supercomputing Center at the University of Alaska, Fairbanks, using the Tsunami Computational Portal at: http://tsunamiportal.nacse.org/wizard.php. The Portal is a joint project of the Northwest Alliance for Computational Science and Engineering at Oregon State University (www.nacse.org) and the Arctic Region Supercomputing Center (www.arsc.edu) at the University of Alaska-Fairbanks.

Grey-shaded relief bathymetry map in Fig. 1 and deep water bathymetry in Fig. 2 are based on multibeam bathymetry with grid resolution of 50 m collected by the University of Madrid using the Simrad EM-120 on the R/V Hesperides in 2005 and by the USGS using SeaBeam 2112 on the NOAA ship Ron Brown in 2006. Low-Resolution bathymetry in Fig. 1 is made from NOAA/NGDC ETOPO1 1 arc-minute grid of global relief data. Shallow water bathymetry is a triangulated irregular network (TIN) of ungridded single-beam bathymetry from NOAA hydrographic surveys distributed by NOAA/NGDC. Color bathymetry is multibeam bathymetry with grid resolution of 5 m collected by the USGS aboard the fishing vessel Tiki XIV in 2009, by Géophysique GPR International, Inc, Montreal, on contract to the University of the Virgin Islands in 2005, and by NOAA Biogeography program aboard the NOAA ship Nancy Foster in 2009.

Grey-shaded relief bathymetry south of Vieques was collected by NOAA Biogeography program aboard the NOAA ship Nancy Foster in 2008 and 2009. LIDAR-based bathymetry around Vieques and Cuelebra were collected by the U.S. Army Corp of Engineers in 2000 using the SHOALS (Scanning Hydrographic Operational Airborne Lidar Survey) system.

Seismic reflection line Sh-24 is part of profile C2124 collected in 1974 by Shell Oil Co. aboard the ship Petrel using a 1200 cu. in airgun array, and a 60-channel, 3000 m long streamer. Line Pe-17 was collected by the USGS aboard the R/V Pelican in 2007 using a 35 cu. in. GI gun, and a 24-channel, 240 m long streamer. Line Ti-8 was collected by the USGS in 2009 aboard the vessel Tiki XIV using a 300 Joule mini-Sparker and a single channel.

Acknowledgments

We thank Tom Logan and Elena Suleimani (Arctic Region Supercomputing Center) and Dylan Keon (Oregon State University) for assistance with running the models. Brian Andrews, Bill Danforth, Chuck Worley, and Emile Bergeron helped with data collection and processing aboard the Tiki XIV and Claudia Flores helped with seismic data processing. Bill Danforth and Brian Andrews merged and gridded the other multibeam bathymetry data. Tim Battista (NOAA) and Ryan Smith (University of the Virgin Islands) provided multibeam bathymetry data on the Virgin Islands platform. Helpful reviews by Eric Geist, Bill Dillon and Bill McCann, and Editor Fred Pollitz are gratefully acknowledged.

References

Aki, K. and P.G. Richards (1980). *Quantitative seismology; theory and methods,* W.H. Freeman, San Francisco.

Barkan, R., U.S. ten Brink and J. Lin (2009). Far field tsunami simulations of the 1755 Lisbon earthquake: Implications for tsunami hazard to the U.S. East Coast and the Caribbean. *Mar. Geol.,* **264** 109-122.

Donnelly, T.W. (1965). Sea-bottom morphology suggestive of post-Pleistocene tectonic activity of the eastern Greater Antilles. *Geol. Soc. Am. Bull.* **76** 1291-1294.

Dookhan, I. (1975). *History of the Virgin Islands*. Univ. of the West Indies Press, Kingston.

Doser, D.I., C.M. Rodriguez, and C. Flores (2005), Historical earthquakes of the Puerto Rico-Virgin Islands region (1915-1963), *Geol. Soc. Am. Spec. Pap.* ***385***, p. 103-114.

Frankel, A., W.R. McCann, and A.J. Murphy (1980). Observations from a seismic network in the Virgin Islands region: Tectonic structure and earthquake swarms. *J. Geophys. Res.* **85** 2669-2678.

Fratantoni, D.M., R.J. Zantopp, W.E. Johns, and J.L. Miller (1997). Updated bathymetry of the Anegada–Jungfern Passage complex and implications for Atlantic inflow to the abyssal Caribbean Sea. *J. Mar. Res.* **55** 847-860.

Gill, I., P.P. McLaughlin, Jr. and D.K. Hubbard (1999). Evolution of the Neogene Kingshill Basin of St. Croix, U. S. Virgin Islands. In *Caribbean basins* P. Mann (Editor), Sedimentary Basins of the World. Elsevier, Amsterdam, pp. 343-366.

Green, G. (1837). On the motion of waves in a variable canal of small depth and width. *Trans. Cambridge Philos. Soc.* **6** 457-462.

452 Hess, H.H. and J.C. Maxwell (1953). Caribbean Research Project. *Geol. Soc. Am. Bull.,*
453 **64** 1-6.
454 Jany, I., K.M. Scanlon, and A. Mauffret (1990). Geological interpretation of combined
455 Seabeam, GLORIA and seismic data from Anegada Passage (Virgin Islands,
456 North Caribbean). *Mar. Geophys. Res.* **12** 173-196.
457 Lander, J.F., L.S.Whiteside, and P.A. Lockridge (2002). A brief history of tsunamis in
458 the Caribbean Sea. *Sci. Tusnami Haz.* **20** 57-94.
459 Liu, P.L.-F., S.-B. Woo, and Y.-S. Cho (1998). *Computer program for tsunami*
460 *propagation and Inundation,* sponsored by National Science Foundation.
461 Lynett, P. J., T.-R. Wu, and P. L.-F. Liu (2002). Modeling wave runup with depth-
462 integrated equations, *Coastal Engineering* **46** 89-107.
463 Macintyre, I.G., B.B. Burke, R.B. and R. Stuckenrath (1977). Thickest recorded
464 Holocene reef section, Isla Perez core hole, Alacran Reef, Mexico. *Geology* **5**
465 749-754.
466 Matsuyama, M., J. P. Walsh, and H. Yeh (1999). The effect of bathymetry on tsunami
467 characteristics at Sissano Lagoon, Papua New Guinea, *Geophys. Res. Lett.* **26**
468 3513-3516.
469 McCann, W.R. (1985). On the earthquake hazards of Puerto Rico and the Virgin Islands,
470 *Bull. Seismol. Soc. Am.* **75** 251-262.
471 Meyerhoff, H.A. (1927). *The physiography of the Virgin Islands, Culebra, and Vieques,*
472 *Scientific Survey of Porto Rico and the Virgin Islands 1926-27,* New York Acad.
473 Sci.

474 Mofjeld, H.O., V.V. Titov, F.I. Gonzalez, J.C. and Newman (2000). *Analytic theory of*
475 *tsunami wave scattering in the open ocean with application to the North Pacific,*
476 NOAA Technical Memorandum OAR PMEL-116.
477 Murphy, A.J. and W.R. McCann (1979). Preliminary results from a new seismic network
478 in the northeastern Caribbean. *Bull. Seismol. Soc. Am.* **69** 1497-1513.
479 O'Loughlin, K.F. and J.F. Lander (2003). *Caribbean tsunamis*. Kluwer Academic
480 Publishers, Dordrecht, 263 pp.
481 Pacheco, L.D. and L.R. Sykes (1992). Seismic moment catalog of large shallow
482 earthquakes, 1900 to 1989. *Bull. Seismol. Soc. Am.* **82** 1306-1349.
483 Reid, H.F. and S. Taber (1920). The Virgin Islands earthquakes of 1867-1868. *Bull.*
484 *Seismol. Soc. Am.* **10** 9-30.
485 ten Brink, U.S. (2005). Vertical motions of the Puerto Rico Trench and their cause. *J.*
486 *Geophys. Res.* **110** B06404, doi:10.1020/2004JB003459.
487 Van Moorsel, G.W.N.M. (1985). Disturbance and growth of juvenile corals (Agaricia
488 humilis and Agaricia agaricites, Scleractinia) in natural habitats on the reef of
489 Curacao. *Mar. Ecology - Progress Series* **24** 99-112.
490 Vaughan, T.W. (1923). Stratigraphy of the Virgin Islands of the United States and of
491 Culebra and Vieques islands, and notes on eastern Porto Rico. *J. Washington*
492 *Acad. Sci.* **13** 303-317.
493 Ward, S. (2002). Tsunamis. *Encyclopedia of Physical Science and Technology* **17** 175-
494 191.
495 Wells, D.L. and K.J. Coppersmith (1994). New empirical relationships among
496 magnitude, rupture length, rupture width, rupture area, and surface displacement.
497 *Bull. Seismol. Soc. Am.* **84** 974-1002.

498 Woodruff, J.D., J.P. Donnelly, D. Mohrig, and W.R. Geyer (2008). Reconstructing
499 relative fl ooding intensities responsible for hurricane-induced deposits from
500 Laguna Playa Grande, Vieques, Puerto Rico, *Geology*, ***36*** 391-394.
501 Zahibo, N., E. Pelinovsky, A. Yalciner, A. Kurkin, A. Koselkov, and A. Zaitsev (2003).
502 The 1867 Virgin Island tsunami; observations and modeling. *Oceanologica Acta*
503 **26** 609-621.
504
505
506 **Figure Captions**
507 Fig. 1. (a) Locations of run-up reports in Table 1. Shaded blue bathymetry- referred to as
508 LRES bathymetry in text. Multibeam bathymetry- referred to as HRES bathymetry in
509 text. Contour interval is 500 m. (b) Bathymetric map of the Virgin Islands and Puerto
510 Rico regions. Earthquake sources (placed in the center of finite faults) used to generate
511 tsunami simulations are shown in red circles with corresponding fault model number (see
512 Table 2 for source coordinates and fault parameters). Locations of detailed near source
513 run-up reports in Table 1 are also shown as green dots. RF- refers to a scarp which may
514 correspond to our hypothesized RF (see section 3.3 for details). VIB- Virgin Island Basin.
515 NF-North Fault (see text for details).
516
517 Fig. 2 – Shaded bathymetry map of the Virgin Islands basin and the Virgin Islands
518 platform. Blue lines – locations of seismic profiles shown at the bottom right corner and
519 in Figure 10. Heavy dashed line – proposed location of the fault rupture of the 1867
520 earthquake and tusnami. Thin dashed lines – Other possible active faults in the area.
521 Dotted line encloses area of morphological disturbance in the basin wall below the

proposed 1867 fault rupture. Brown area at the eastern end of Vieques – Uplifted and tilted Pleistocene(?) platform (Meyerhoff, 1926). Black rectangle – Location of dive. Yellow star – Location of earthquake swarms in 1978-1979 (Frankel et al., 1980). NF, RF, and ZF, are the central locations of fault sources used in the tsunami simulations: North Fault, Reid Fault, and Zahibo Fault. DF – Fault trace proposed by Donnelly (1965). Top right inset – Dive along the proposed fault scarp by Donnelly (1965). Note that the slope is covered by well-developed lettuce corals. Photo taken by Drex Harrington. Bottom right inset – Part of single-channel seismic line Ti-2 collected by a mini-sparker in 2009. Note lack of offset along the proposed fault by Donnelly (DF). Top left inset – Enlargement of the multibeam bathymetry in the region marked by an open black rectangle. LPG – Location of Laguna Playa Grande where Woodruff et al. (2008) did not find distinct tsunami deposits from 1867.

Fig. 3. X^2 comparison between fault sources that vary in (a) longitude, and (b) latitude. Location of sources is shown in Figure 2 and listed in Table 2. Smaller bars represent sources that are better fitting to be the 1867 Virgin Island epicenter (see section 2.3 for explanation). According to this test source 7 (Long -65°E) is the best fitting candidate in longitude and locations between source 14 (Lat 18.1667°N) and source 20 (Lat 18.3°N) are the best fitting candidates in latitude.

Fig. 4. X^2 comparison between tsunami amplitudes for different fault parameters located in source 14 (see Fig. 2 and Table 2). The parameters include (a) variations in fault strike, (b) combinations of fault dimensions (length x width x slip), and (c) rake. Smaller bars represent fault parameters that are better fitting to be the 1867 Virgin Island fault

parameters (see section 2.3 for explanation). According to this test strikes ranging from 120°-140°, had a combined Left Lateral (LL) and Normal (N) slip with a rake of -45° and an earthquake with a relatively small area and relatively large slip (combination # 3) best describes the 1867 VI earthquake. R – Reverse slip.

Fig. 5. X^2 comparison between our best overall candidates RF and NF, and ZF (Zahibo et al., 2003) (see Table 3).. Smaller bars represent fault candidates that are better fitting to be the 1867 Virgin Island fault (see section 2.3 for explanation). According to this test RF and NF are clearly better fitting than ZF (see section 3.3 for detail). Furthermore, SE trending faults (strikes 120° and 135°) are a better fit, suggesting a drop in the SW side of the fault.

Fig. 6. Maximum wave amplitude from an earthquake source located in RF (see source 14 in Fig. 2 and Table 3 for fault parameters). a) Entire region of study. b) Region of Puerto Rico and the Virgin Islands. The scale ranges from 0-2 m. VI- Virgin Islands.

Fig. 7. Marigrams from RF (See table 3), computed at several coastal locations described in Table 1 and shown in Figure 1 (horizontal axis is the time and vertical axis is water surface elevation). As can be seen the leading propagating wave in all sites is a depression phase, in agreement with historical reports. The amplitudes of the marigrams were calculated at the centers of the crosses at the coordinates given in Table 1. The amplitudes of the marigrams were NOT normalized to water depth using Green's Law.

569 Fig. 8. Marigrams from NF (See table 3), computed at several coastal locations described
570 in Table 1 and shown in Figure 1 (horizontal axis is the time and vertical axis is water
571 surface elevation). As can be seen the leading propagating wave in all sites is a
572 depression phase, in agreement with historical reports.
573 .
574 Fig. 9. Same as Fig. 7, but with a strike of 300°. As can be seen the leading propagating
575 wave in all sites is a depression phase, in agreement with historical reports. Note the
576 depression forming at the time of the rupture on the Marigram of St. Thomas. This is
577 because St. Thomas is <25 km from the rupturing fault and the NW side of the fault is
578 assumed to subside in this model. Reid and Taber (1920) quote two U.S. Navy
579 eyewitness reports observing the water to have rushed out immediately after the first
580 shock.
581
582 Fig. 10. Seismic profiles crossing the proposed rupture of the 1867 earthquake and
583 tsunami (see Figure 2 for location). The difference in resolution and penetration between
584 the lines is due to different sound sources (see data and resource section).

Table 1- Sites of historical 1867 tsunami run-up reports

Site		Reported Run-up (m)	Relative Amp.		j	Calc. Location		Sources	Travel Time (min)	
			X^2	Calc.		Long (°E)	Lat (°N)		Rep.	Calc.
St. Thomas	Hassel Island	4.9	1	1.462	0	-64.933	18.27	Za, Rei	0-10	9
	Charlotte Amalie	6				-64.953	18.315	Za, Rei		
St. Croix	Frederiksted	7.6				-64.886	17.708	Za, Rei	0-10	4
	North West		1.2667	1.613	1	-64.87	17.782			
Puerto Rico	Vieques	High Waves				-65.382	18.095	Za, Rei	0	
	Culebra					-65.29	18.26	OL, Rei		
	Arroyo	1.5				-66.064	17.91	OL, Za, Rei		
	Salinas					-66.285	17.87	OL		
	Yabucoa	2 (IH)	0.333	0.382	2	-65.818	18.007	Za, Rei		11
	Fajardo	Very small				-65.833	18.001	Rei		
British VI	Virgin Gorda					-64.444	18.402	OL		
	Peter Island	1.5	0.3	0.596	3	-64.581	18.322	Za, Rei		7.5
	Tortola*	1.5				-64.647	18.32	Za, Rei		
Leeward Islands	St. Martin					-63.075	18.017	OL		30.5
	St. Bart					-62.88	17.875	OL, Rei		
	Saba	High Waves				-63.254	17.635	Za, Rei		
	Barbuda	1.4	0.28	0.390	**4**	-61.9	17.626	OL		58
	St Kitts	2.4	0.48	0.436	**5**	-62.8	17.337	OL, Za		
	Montserrat					-62.24	16.78	OL		
	St. John's, Antigua	3 (IH)	0.5	0.386	**6**	-62	17.119	Za, Rei		61.5
Guadeloupe	Basse Terre	2	0.4	0.415	**7**	-61.712	15.993	Za, Rei	0-10	
Dominica	Prince Rupert's bay	3				-61.476	15.56	OL		59
Martinique		Reported								73
St. Lucia	Anse la raye	1.2				-61.062	13.938	Za, OL		
St. Vincent	Cumberland bay	0.6	0.12	0.404	**8**	-61.3	13.255	OL		78
Grenadines	Admiralty bay	1.8	0.333	0.416	**9**	-61.31	13	Za, OL		
Grenada	St. George's	1.5	0.3	0.512	**10**	-61.77	12.119	Za, Rei	120 - 140	84
Venezuela	Isle de Margarita	Reported				-64	11.226	Za, Rei		

Run-up reports are from Reid and Taber, 1920 (Rei); Zahibo et al., 2003 (ZA); O'Loughlin and F. Lander, 2003 (OL).
Relative amplitude (X^2) for X^2 analysis is normalized to St. Thomas, outside the harbor (see section 2.3 for details). Relative amplitude (Calc.) is from RF (see section 3.3 for details).
Column 'j' depicts the historical sites that were used for X^2 analysis (see section 2.3 for details): Shaded gray numbers and bold numbers are in areas of high-resolution (HRES) and low-resolution (LRES) bathymetric grid, respectively (see section 2.1 for details).
The coordinates (long. and lat.) indicate the center of the group of grid points where the amplitude was calculated (see section 2.2 for details).
Travel time-first arrival phase after estimated time of earthquake (see section 3.4 for details) Rep. for reported, Calc. for calculated.
Tortola* - The calculated point for Tortola is between St. John, USVI, and Peter Island, because the numerical model could not propagate the tsunami through the shallow water and dispersed islands.
IH-In Harbor.

Table 2- Geographical coordinates and fault parameters of source locatioas shown in figure 2

Source	Long (°E)	Lat (°N)	Length (km)	Width (km)	Slip (m)	Strike (°)	Rake (°)	Dip (°)
1	-65.5259	17.735	80	35	2	110	-90	60
2	-65	17.85	60	25	5	75	-90	45
3	-65.2463	17.90417	80	35	2	110	-90	60
4	-65	17.9167	varying	varying	varying	varying	varying	varying
5	-65	17.9667	80	35	2	110	-90	60
6	-64.6972	17.9833	80	35	2	110	-90	60
ZF (7)	-65	18	varying	varying	varying	varying	varying	varying
8	-65	18.02	60	35	2.667	all	-90	60
9	-64.8543	18.02783	80	35	2	110	-90	60
10	-64.419	18.031	80	35	2	110	-90	60
11	-64.9	18.052	60	25	5	110	-90	45
12	-65.498	18.061	60	25	5	78	-90	45
13	-65.222	18.12	60	25	5	75	-90	45
RF (14)	-65	18.1667	varying	varying	varying	varying	varying	varying
15	-64.705	18.194	60	25	5	78	-90	45
NF (16)	-65	18.2	varying	varying	varying	varying	varying	varying
17	-65	18.23	60	25	5	75	-90	45
18	-65	18.25	80	35	2	110	-90	60
19	-65	18.265	80	35	2	110	-90	60
20	-65	18.3	80	35	2	110	-90	60
21	-64.462	18.335	60	25	5	110	-90	45

Source locations are measured in the center of each finite fault.
Source depth for all faults is 1000m, taken at the top of the fault plane.

Table 3

Table 3- Epicenter location and fault parameters for the best fitting candidates and Zahibo Fault

Fault	Long (°E)	Lat (°N)	Length (km)	Width (km)	Slip (m)	Strike (°)	Rake (°)	Dip (°)	X^2 Far	X^2 Close	X^2 Total
NF	-65	18.2	50	25	6	135/315	-45	45	0.4087	0.1325	0.5412
RF	-65	18.167	50	25	6	120/300	-45	45	0.4337	0.0753	0.509
ZF	-65	18	50	25	6	75/255	-45	90	0.3309	0.3772	0.7081

NF- North Fault.
RF - Reid Fault.
ZF –Zahibo Fault.
Source locations are measured in the center of each finite fault.
Source depth for all faults is 1000m, taken at the top of the fault plane.
The dimensions of ZF were reduced to fit the hypothesized M7.5.

Figure 1

Click here to download high resolution image

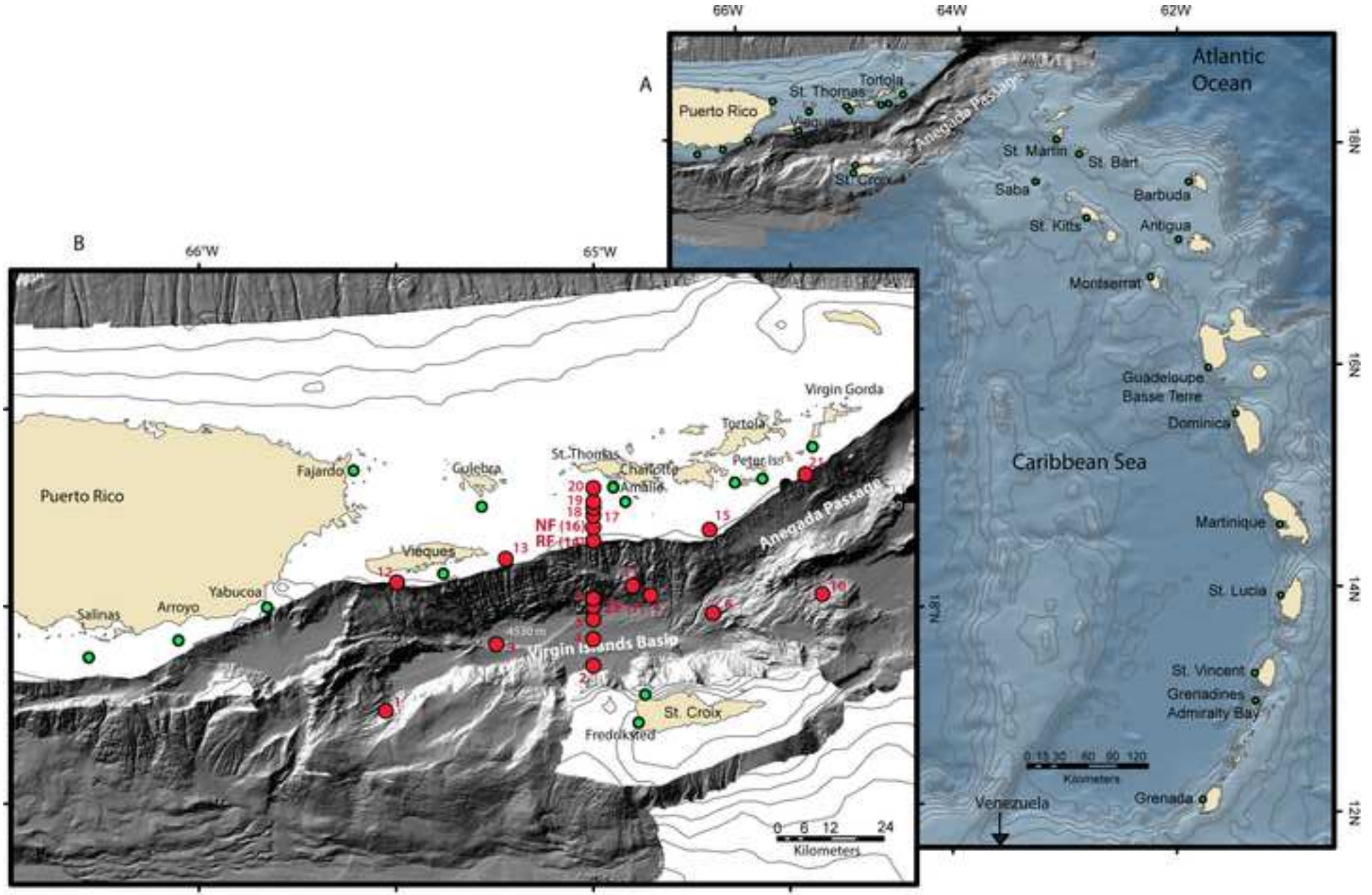

Figure 2

Click here to download high resolution image

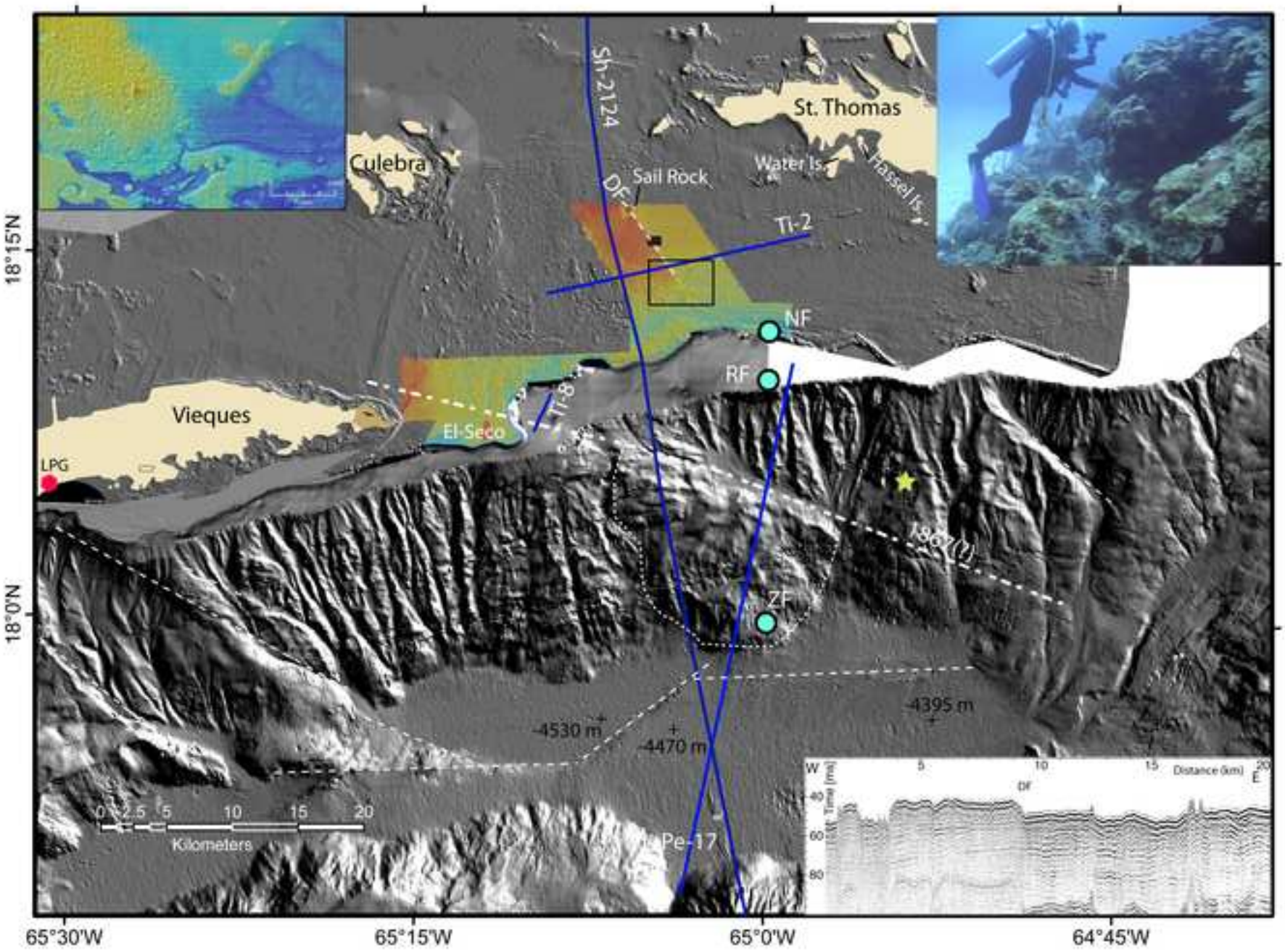

Figure 3

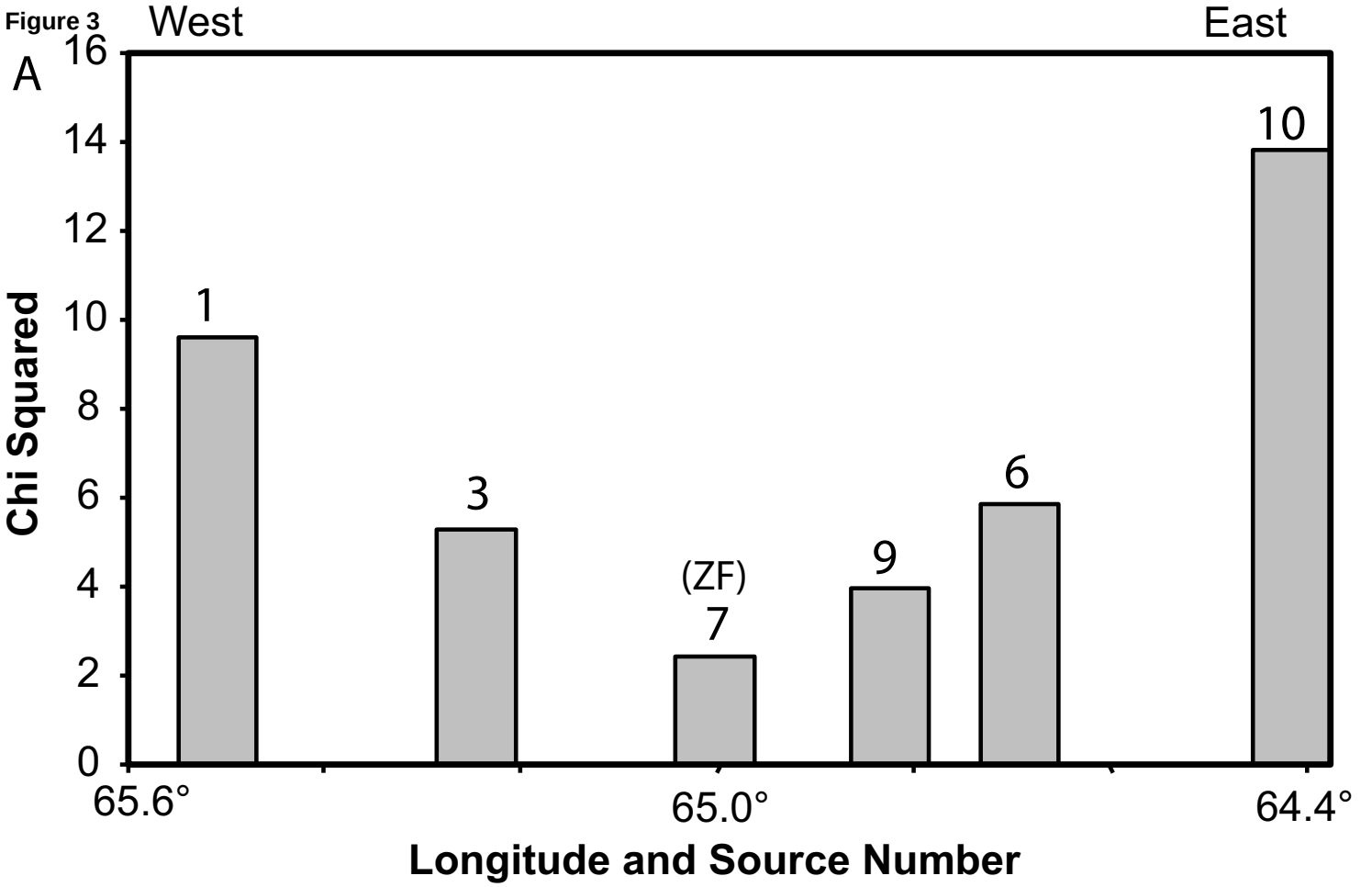
A
West
East
16
14
12
10
8
6
4
2
0
Chi Squared
1
3
(ZF)
7
9
6
10
65.6°
65.0°
64.4°
Longitude and Source Number

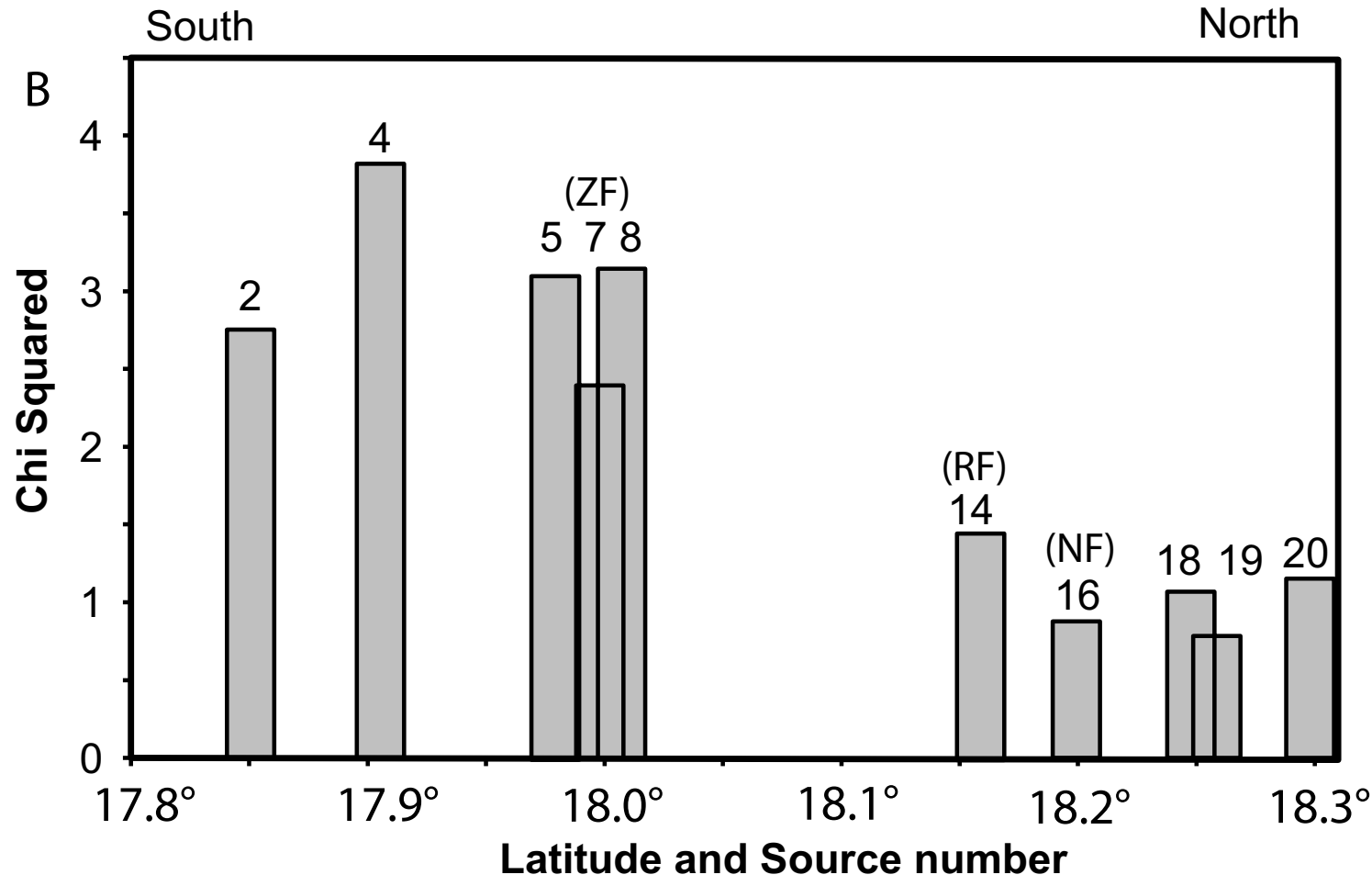
B
South
North
4
3
2
1
0
Chi Squared
4
(ZF)
5 7 8
2
(RF)
14
(NF)
16
18 19 20
17.8°
17.9°
18.0°
18.1°
18.2°
18.3°
Latitude and Source number

Figure 4 a,b,c

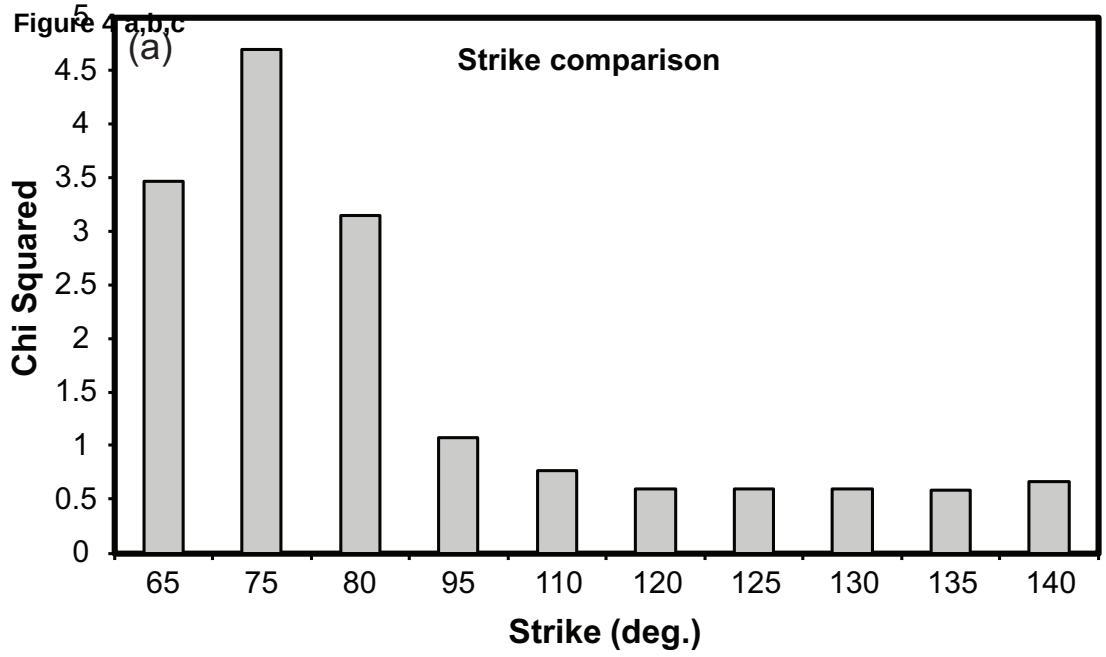
(a)
Strike comparison
Chi Squared
5
4.5
4
3.5
3
2.5
2
1.5
1
0.5
0
65
75
80
95
110
120
125
130
135
140
Strike (deg.)

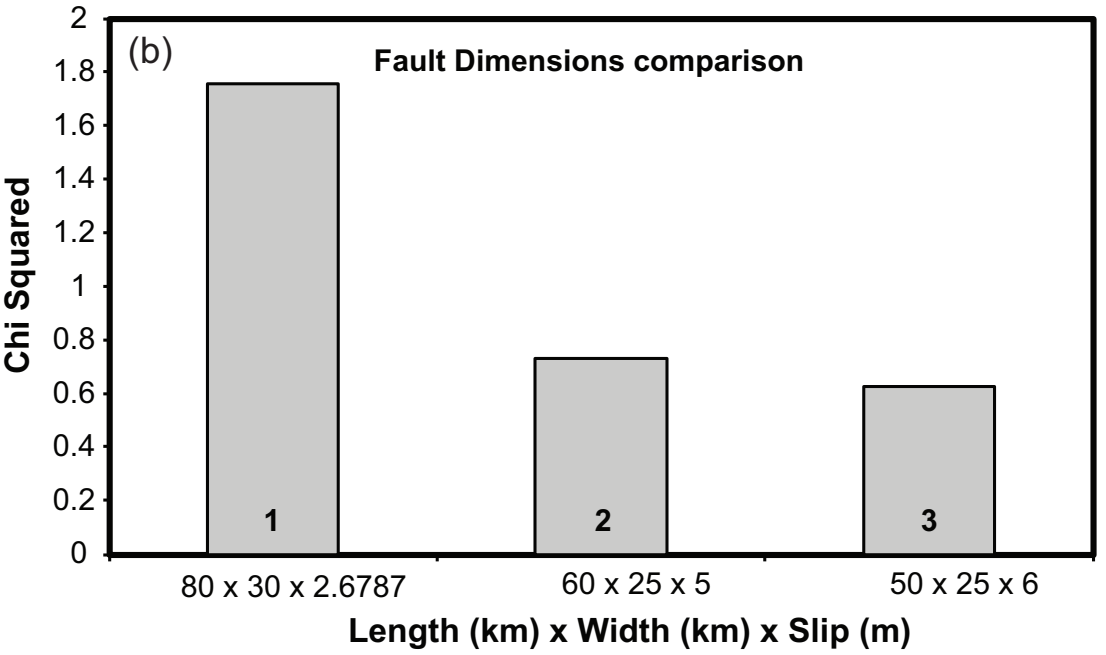
(b)
Fault Dimensions comparison
Chi Squared
2
1.8
1.6
1.4
1.2
1
0.8
0.6
0.4
0.2
0
1
2
3
80 x 30 x 2.6787
60 x 25 x 5
50 x 25 x 6
Length (km) x Width (km) x Slip (m)

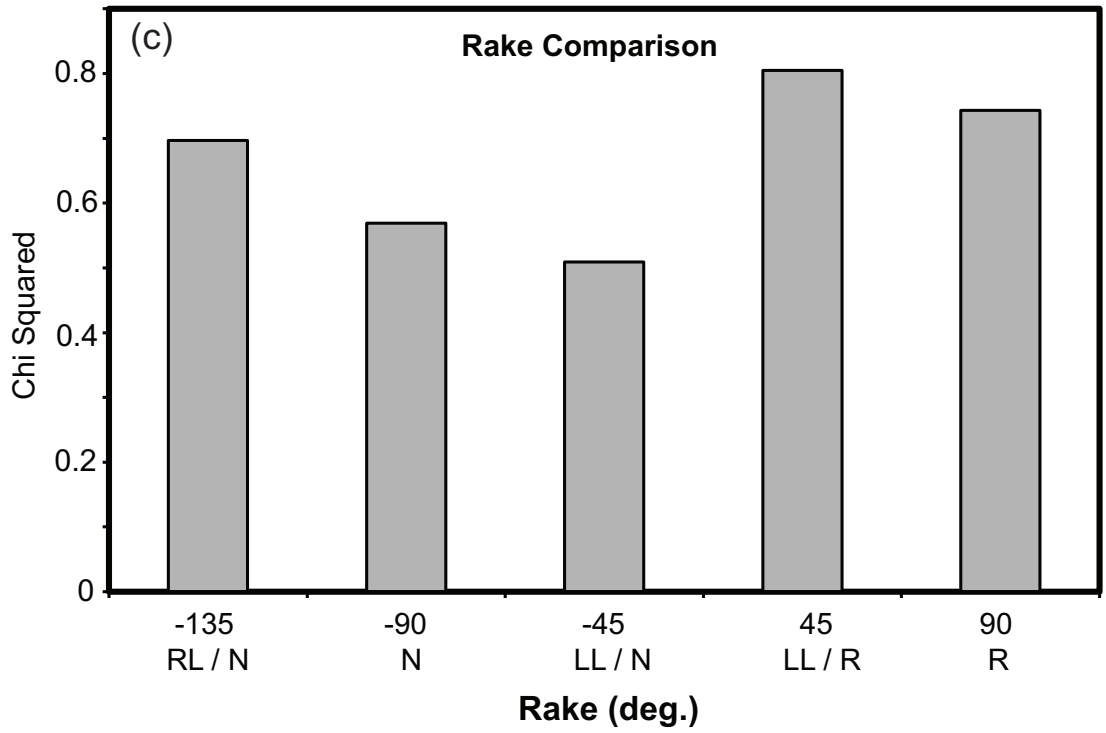
(c)
Rake Comparison
Chi Squared
0.8
0.6
0.4
0.2
0
-135
RL / N
-90
N
-45
LL / N
45
LL / R
90
R
Rake (deg.)

Figure 5

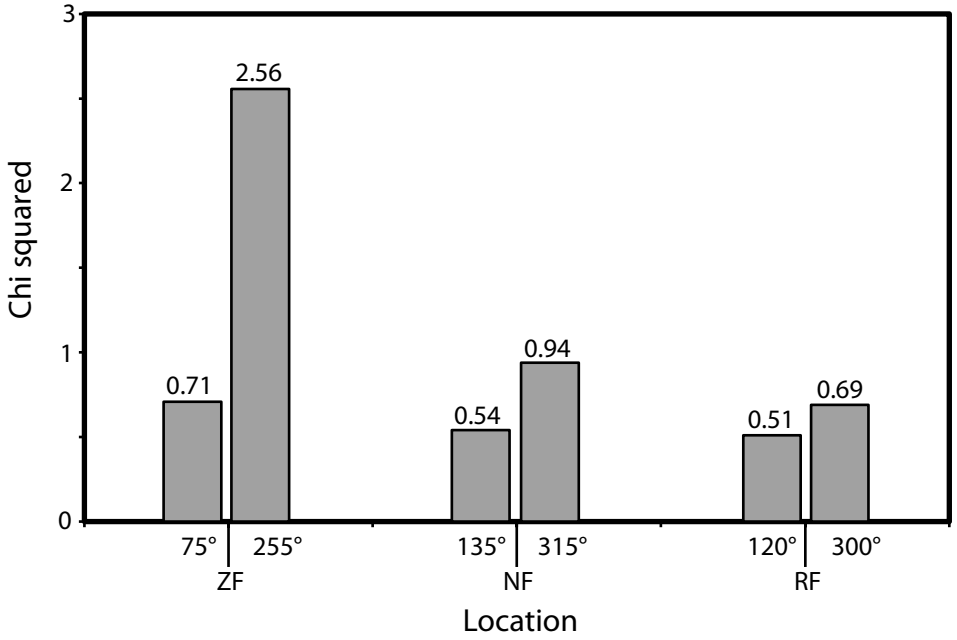
3
2
1
0
Chi squared
2.56
0.71
0.94
0.54
0.69
0.51
75°
255°
135°
315°
120°
300°
ZF
NF
RF
Location

Figure 6

Click here to download high resolution image

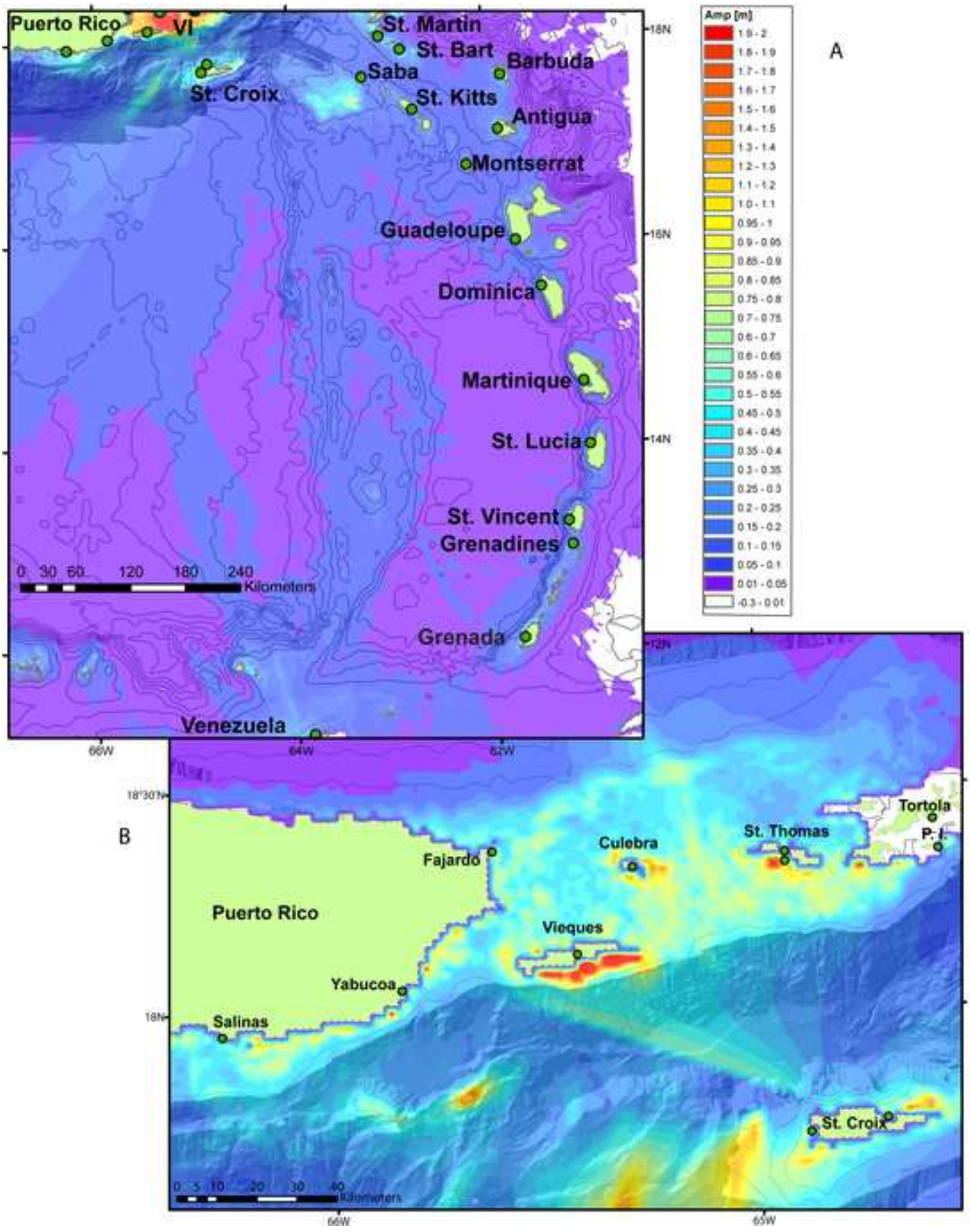

Figure 7

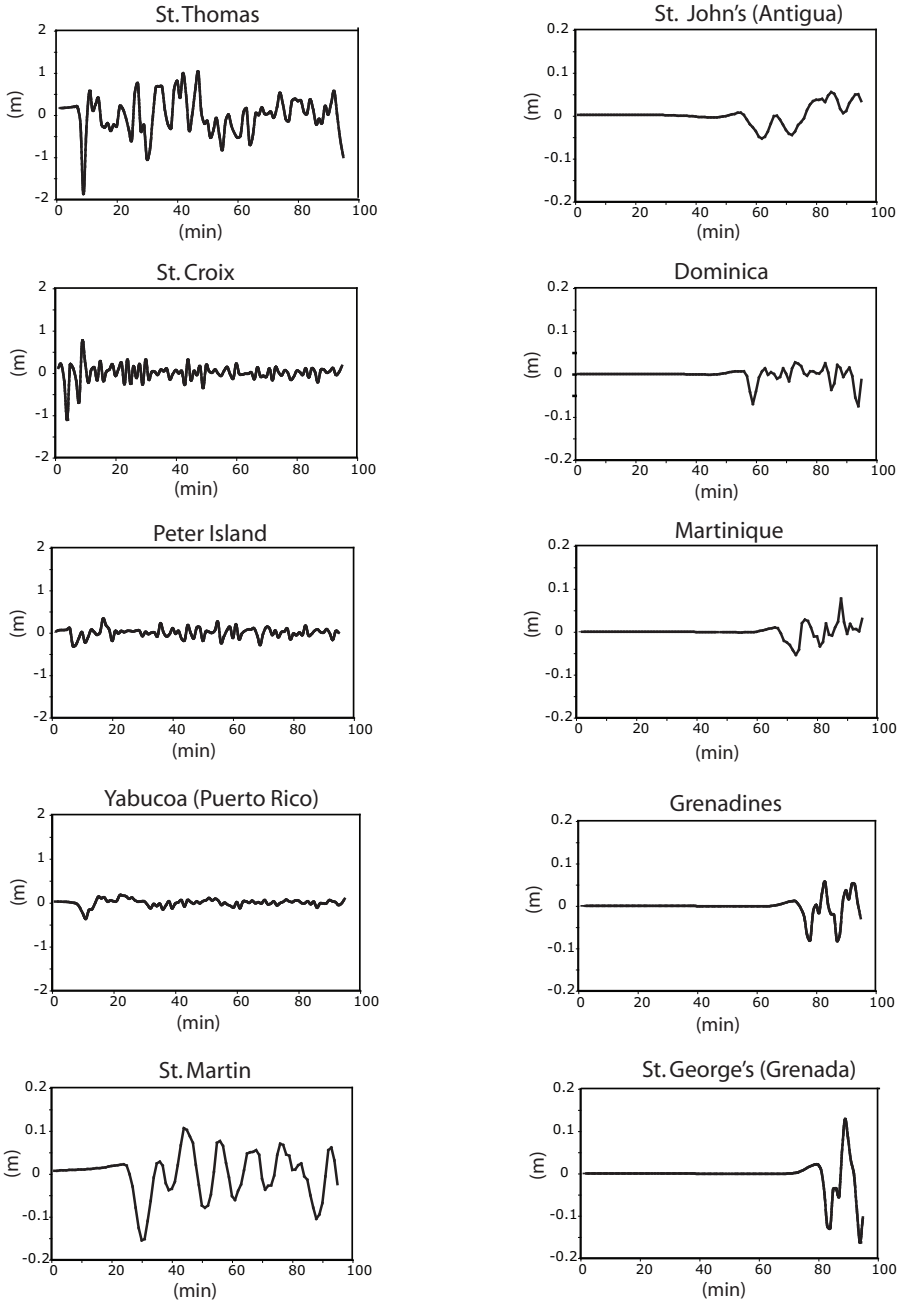
St. Thomas
St. John's (Antigua)
St. Croix
Dominica
Peter Island
Martinique
Yabucoa (Puerto Rico)
Grenadines
St. Martin
St. George's (Grenada)
(m)
(min)

Figure 8

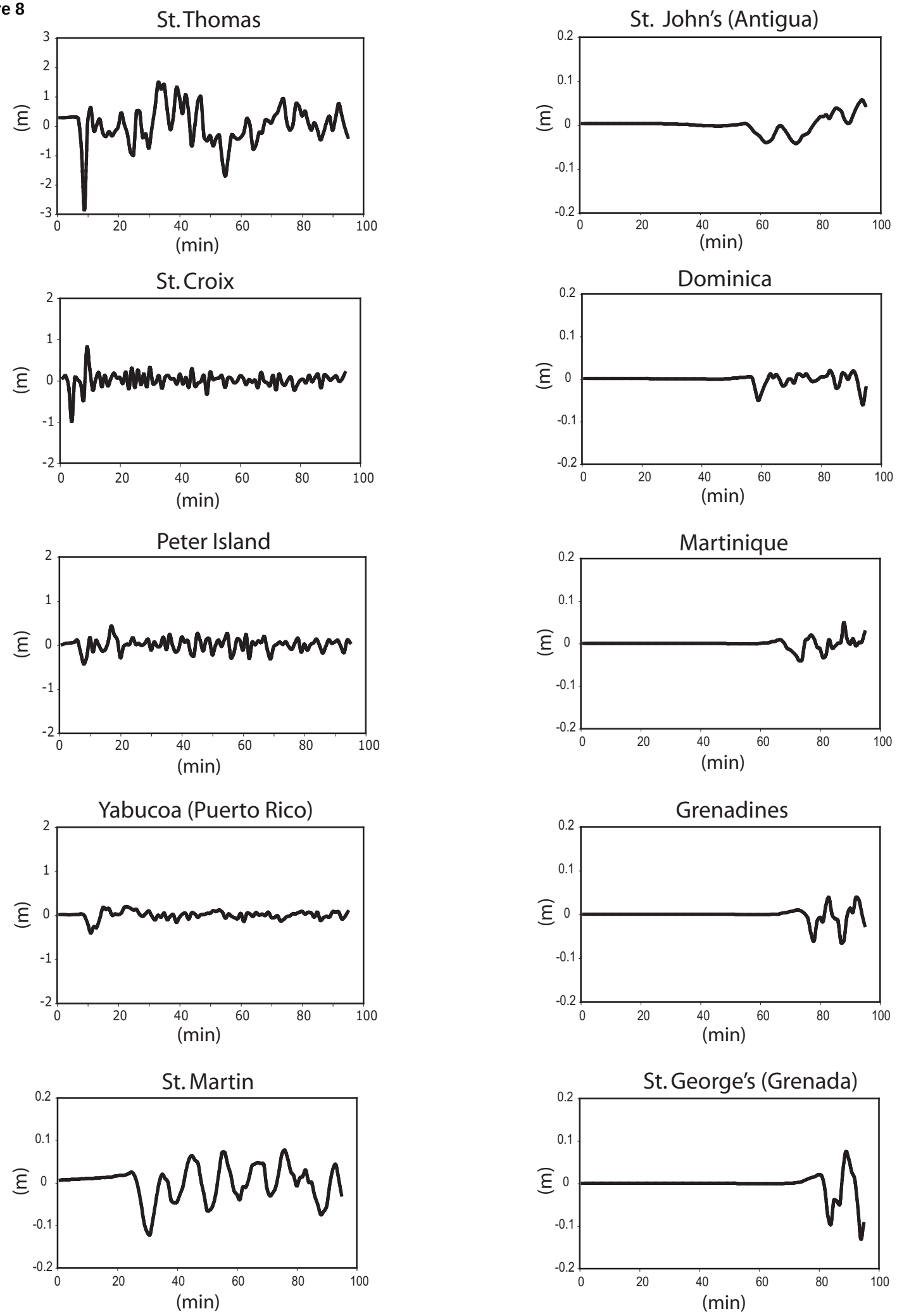
St. Thomas
St. John's (Antigua)
St. Croix
Dominica
Peter Island
Martinique
Yabucoa (Puerto Rico)
Grenadines
St. Martin
St. George's (Grenada)
(m)
(min)

Figure 9

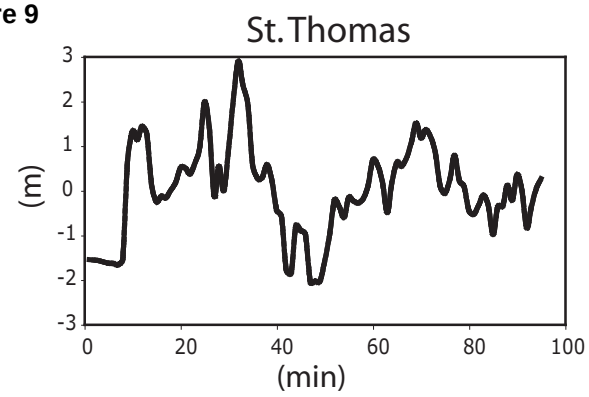
St. Thomas
(m)
(min)

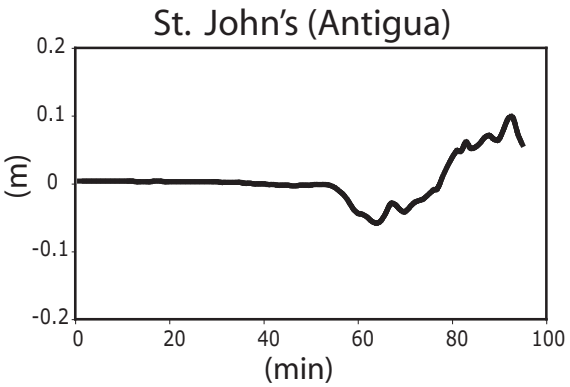
St. John's (Antigua)
(m)
(min)

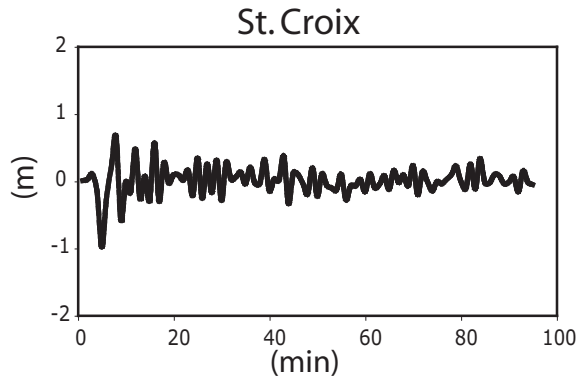
St. Croix
(m)
(min)

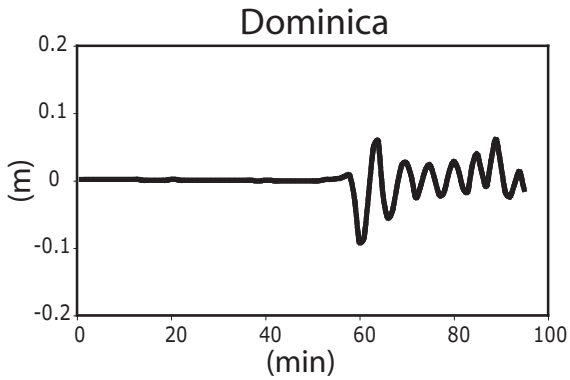
Dominica
(m)
(min)

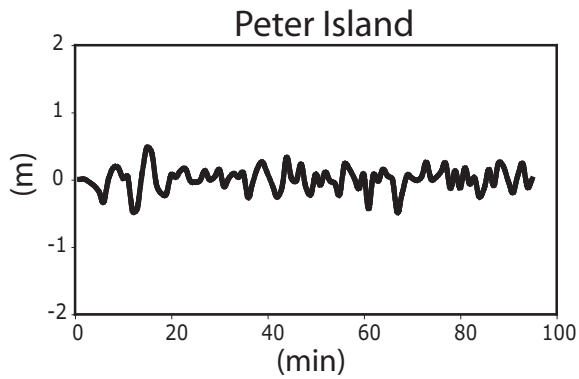
Peter Island
(m)
(min)

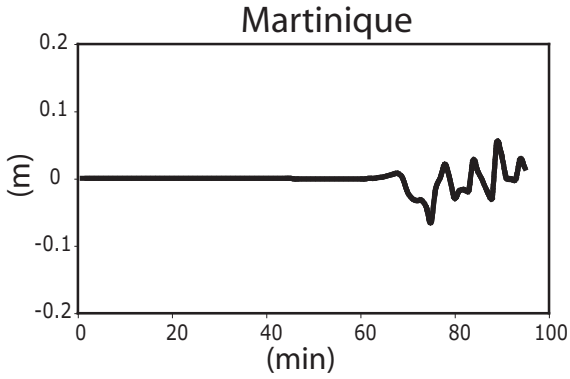
Martinique
(m)
(min)

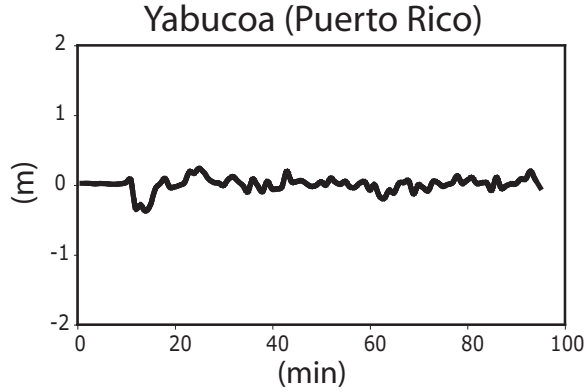
Yabucoa (Puerto Rico)
(m)
(min)

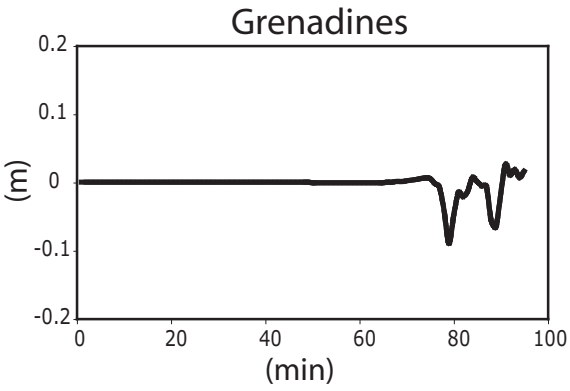
Grenadines
(m)
(min)

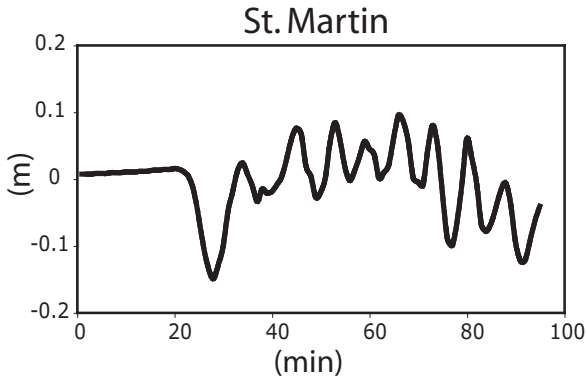
St. Martin
(m)
(min)

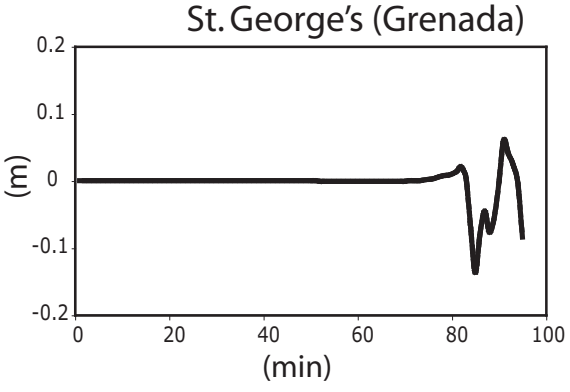
St. George's (Grenada)
(m)
(min)

Figure 10

Click here to download high resolution image